Seatific, Vol. 4, Issue. 1, pp. 12–23, June 2024

Seatific Journal
https://seatific.yildiz.edu.tr
DOI: https://doi.org/10.14744/seatific.2024.0002

Seatific

Research Article

Analyzing tandem effects in oscillating water column WEC arrays: A numerical study of diverse geometries and inter-device gaps

Burcu ÖZSELEK*, Yonglai ZHENG

Department of Hydraulic Engineering, Tongji University, Faculty of Civil Engineering, Shanghai, China

ARTICLE INFO

Article history
Received: April 15, 2024
Revised: May 05, 2024
Accepted: May 12, 2024

Key words:
Oscillating water column; WEC array; tandem effect; numerical simulation; efficiency

ABSTRACT

The utilization of wave energy holds significant promise as a renewable energy source, with Oscillating Water Column (OWC) wave energy converters (WECs) being one of the most established technologies in this field. This study examines the influence of various spacing configurations and different shapes for OWCs on device-device interaction, aiming to assess their impact on hydrodynamic performance. The study employs a fully nonlinear 3D computational fluid dynamics (CFD) model based on Reynolds-averaged Navier–Stokes (RANS) equations and a volume-of-fluid (VOF) surface-capturing scheme to conduct numerical analyses of six array cases using Star CCM+. To refine the free surface wave representations, the adaptive mesh refinement (AMR) technique is employed, thus ensuring accuracy. The model has been rigorously validated against published physical measurements encompassing chamber vertical velocity and chamber differential air pressure. After validation, a series of simulations was conducted to explore the effects on hydrodynamic performance from two key factors of array layout: device spacing and shape. These investigations reveal significant influences on wave power and device efficiency. By providing insight into the complex dynamics among array geometries, spacing arrangements, and energy extraction, this study pushes the boundaries of wave energy conversion research, offering valuable insights for future design and implementation strategies.

Cite this article as: Özselek B, Zheng Y. Analyzing tandem effects in oscillating water column WEC arrays: A numerical study of diverse geometries and inter-device gaps. Seatific 2024;4:1:12–23.

1. INTRODUCTION

In the pursuit of sustainable energy sources, ocean waves are viewed as a vast and largely untapped reservoir of potential. Among the technologies aimed at harnessing this resource, Oscillating Water Column (OWC) wave energy converters (WECs) have received significant attention due to their inherent simplicity, reliability, and environmental compatibility. These devices utilize the oscillating motion of water columns induced by wave action to drive air turbines and generate electricity.

For more than two centuries, inventors have been developing various systems to harness wave power inspired by the energy of ocean waves (Drew et al., 2009; Falcão, 2010; Falnes, 2007; López et al., 2013) .The first recorded patent on wave power technology was filed in 1799 by the father-and-son team of Girard in Paris; however, information about this patent is inaccessible. In the words of Girard, the structure worked by "floating on the sea" (Ross, 2012). Yoshio Masuda, a navy officer from Japan, has been recognized as a pioneer in modern wave energy technology since the 1940s. He developed a floating OWC, a buoy that harnessed wave energy using an air turbine (Falcão & Henriques, 2016).

The 1973 oil crisis prompted a significant shift towards renewable energy sources, increasing interest in large-scale

***Corresponding author.**
*E-mail address: burcuozselek@tongji.edu.cn

wave energy production. Numerous European countries, particularly the United Kingdom, Norway, and Sweden, conducted extensive investigations into the feasibility of wave energy utilization (Falnes, 2007). Research focused on the two-dimensional motion of waves by considering vertical flat plates as obstacles and developed an asymptotic theory based on wave transmission and reflection (Evans, 1978; Newman, 1974). Studies also examined the efficiency of wave energy absorption by OWCs while building upon the prior research by Newman (1974) and Evans (1978). By the early 1990s, most wave energy research in Europe was largely academic (Falcão, 2010). In 1991 the European Commission's decision about doing research and development in renewable energies significantly improved the status of research and development projects for renewable energy, including wave energy. This decision led to an increase in projects and conference papers related to wave energy in Europe (Falcão, 2010). Interest in wave energy also has also grown in the United States and Canada in recent years. Research on wave energy absorption can be conducted theoretically, numerically, or experimentally using physical wave basin or wave flume models. Detailed information about various research studies in this field can be found in the following cited review papers (Drew et al., 2009; Falcão, 2010; Falcão and Henriques, 2016; Falnes, 2007; López et al., 2013; Qiao et al., 2020; Baudry et al., 2013; Windt et al., 2018; Yacob et al., 2022; Zhang et al., 2021).

While individual OWC units have shown promising performance, their integration into arrays offers the potential for enhanced efficiency, scalability, and cost-effectiveness. Extensive arrays of devices are necessary to allow wave energy to make a substantial impact on expansive electric grids (Falcão, 2002). Hence, array configurations present unique opportunities and challenges, including space optimization, layout, and inter-device interactions for maximizing power extraction while minimizing environmental impact. The main challenge for an array of OWC WECs is the hydrodynamic interaction between the devices. Possessing a comprehensive knowledge of these interrelations is crucial for being able to develop hydrodynamically effective and structurally reliable OWC WECs. Initial investigations into the hydrodynamic interaction between devices focused on the theoretical study of oscillating bodies (Budal, 1977; Evans, 1979). Subsequent research by Evans (1982) expanded upon the research by examining oscillating pressure distributions. Infinite-row OWCs within a channel were investigated by Malmo and Reitan (1985). In 2002, Falcão (2002) examined the effects of an infinitely periodic array of non-scattering OWCs on energy absorption using the principles of linear water-wave theory. Nader et al. (2012) developed a novel finite element model to study how wave interactions impact power capture efficiency within finite arrays of fixed cylindrical OWC devices based on linear potential theory. Subsequently, the model was used to analyze the effects of varying spacing and incident wave direction on power capture efficiency. Konispoliatis and Mavrakos (2016) created a novel analytical approach for addressing diffraction alongside the motion and pressure-driven radiation challenges that surround a group of vertical axisymmetric OWCs. O'Boyle et al.'s (2017) experimental study explored the phenomenon of wave fluctuations surrounding arrays of OWC WECs. Their study also looked into the effects of radiated and scattered waves on these arrays. Another experimental study by Doyle and Aggidis (2021) utilized a novel efficient bidirectional airflow, capturing experimental modeling technique to evaluate the effectiveness of various configurations of wave energy converters (e.g., OWC, OWC array, and modular OWCs [M-OWC]) in uniform environmental settings. By varying such parameters as OWC spacing, damping, and wave conditions, their study evaluated and analyzed the performance and responses of these converters. They conducted numerical investigations using the time-domain higher-order boundary element method (HOBEM), which had previously been utilized in Ning et al.'s (2015) study on OWC modeling. This method was further employed recently in numerical and experimental research (Zhou et al., 2020; Zhou et al., 2021) focused on a cylindrical-shaped multifunctional OWC structure within a 3D nonlinear numerical wave tank (NWT). Subsequently, Zhou et al. (2022) extended the research to explore the array layout of a quad-cylindrical type OWC configuration. Factors such as wave direction and spacing were taken into account while utilizing a 3D nonlinear time-domain HOBEM. Manimaran (2024) carried out a tandem effect study numerically to observe the effects of pressure drop and efficiency on the performance of a multi-rectangular OWC chamber and a trapezoidal OWC chamber. Nevertheless, implementing multiple OWCs under actual sea conditions still needs to be developed worldwide. This is primarily due to the deficiency of experimental and numerical OWC array studies. Both types of studies are expensive, but advancements in technology may help overcome these obstacles.

This study aims to explore the behavior of multiple OWCs in a specific marine environment under wave tank settings. The research involves analyzing six scenarios, which include different distance widths as well as geometries with consistent widths and diameters. The investigation focuses on comparing the speeds, average power outputs, and efficiencies of the different OWC configurations. This study provides a different perspective by examining how varying spacing and shapes in relation to device width impacts the performance of OWC arrays. This research uses an in-depth computational fluid dynamic (CFD) analysis with the goal of enhancing understanding in the field of wave energy conversion and provide valuable insights for the design and implementation of OWC WEC layouts.

2. CFD MODELING

2.1. Computational framework and equations

The study configures the hydrodynamic model to represent the viscous incompressible flow field surrounding OWCs

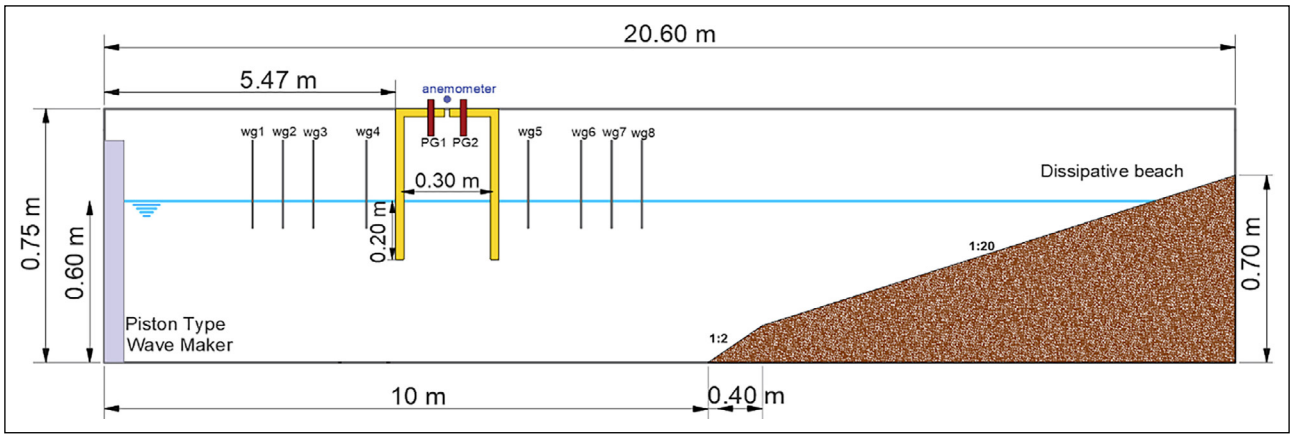

Figure 1. Iturrioz et al.'s experimental study setup (modified drawing from (Iturrioz et al., 2015)).

and subject to the governing Reynolds-averaged Navier-Stokes (RANS) and continuity equations. The free surface is simulated using the volume of fluid (VOF) solver method inspired by Hirt & Nichols' (1981) study. The high-resolution interface capturing (HRIC) method was executed within a 3D computational model. Because the κ-ω shear-stress transport (SST) model offers accurate predictions for simulating flow separation in adverse pressure gradients, turbulence in the flow field was represented using the κ-ω SST equations. The turbulent kinetic energy (κ) and specific dissipation rate (ω) are addressed through the dual-equation model established by Siemens Digital Industries Software (2020).

The governing equations can be expressed as follows:

$$\frac{\partial u_i}{\partial x_i} = 0 \tag{1}$$

$$\rho\left(\frac{\partial u_i}{\partial t} + u_j\frac{\partial u_i}{\partial x_j}\right) = -\frac{\partial p}{\partial x_i} + \frac{\partial}{\partial x_j}\left(\mu\frac{\partial u_i}{\partial x_j} - \rho\overline{u_i' u_j'}\right) \tag{2}$$

where u_i represents the velocity measured over time, p, ρ, and μ represent the pressure, density, and dynamic viscosity, respectively. The Reynolds stress tensor, which captures the impact of turbulence on the mean momentum, is contributed by the final element on the right-hand side of Eq. 2.

The research employs numerical simulations utilizing the Eulerian multiphase model to simulate two distinct phases: air and water. The monitoring of free fluid surfaces was achieved through the Waves model within the Simcenter Star CCM+ software. The governing equations have been discretized using the finite volume method (FVM) to improve solution accuracy. A second-order scheme was employed for both the temporal and spatial discretization. The velocity-pressure coupling was achieved using the SIMPLE algorithm. The simulation duration was set at 90 s, with a time step of 0.01 s for each iteration.

The properties of the numerical environment were characterized by the density and kinematic viscosity values for air (ρ_0=1 kg/m^3, ν=1.48 × 10^{-5} m^2/s) and water (ρ_w=1000 kg/m^3, ν=10^{-6} m^2/s).

2.2. Creating the domain

The CFD model has been constructed based on the experimental parameters outlined by Iturrioz et al. (2015). According to test tank set-up (see Iturrioz et al., 2014, 2015), wave flume length is 20.60 m, width is 0.68 m and height is 0.75 m. A beach located 10 m away from the wave-maker with a draught of 0.20 m serves to minimize wave reflections. Two pressure gauges (PG1 and PG2) are situated in the top section of the chamber. The schematic representation of the wave flume was adapted from Iturrioz et al. (2015) and is depicted in Figure 1. The NWT has been created in Simcenter Star CCM+. Iturrioz et al. (2015) explored various top slot scenarios, wave heights, and wave periods. The current study focuses on simulating Case C24 with a 9mm top slot scenario, as this demonstrates superior performance and achieves optimal efficiency. After validating the numerical setup of a single rectangular OWC, six unique array configurations have been systematically organized and evaluated for power efficiency.

2.3. Boundary conditions

The computations are carried out using a Cartesian coordinate framework, with the point of origin located at the intersection of the model. The positive x-axis and upward-pointing positive y-axis indicate the direction of the entering flow. The waves are propagating in the positive x direction. Carefully selecting appropriate boundary conditions is imperative for achieving accurate modeling of free surface flows. The created wave tank is 10 m long, so it ends right before the dissipative beach. The inlet and outlet boundaries are placed on the left and right sides of the tank, respectively. The OWC model is situated 5.47 m from the inlet boundary, and a uniform velocity is applied from this side. The outlet boundary is pressure, and the remaining walls are subject to a no-slip boundary constraint. The numerical wave tank sketch and model view of the OWC are shown in Figure 2.

2.4. Array configurations for the OWCs

This study employs three different geometries of OWC WECs, each evaluated at two different inter-WEC distances. As a result, a total of six unique configurations have been examined. The inter-device distances have been studied as 10 times and 5 times the width, which is represented as the diameter (D) of the WEC, and was held constant at 0.34 m for all cases. Table 1 provides an overview of each configuration.

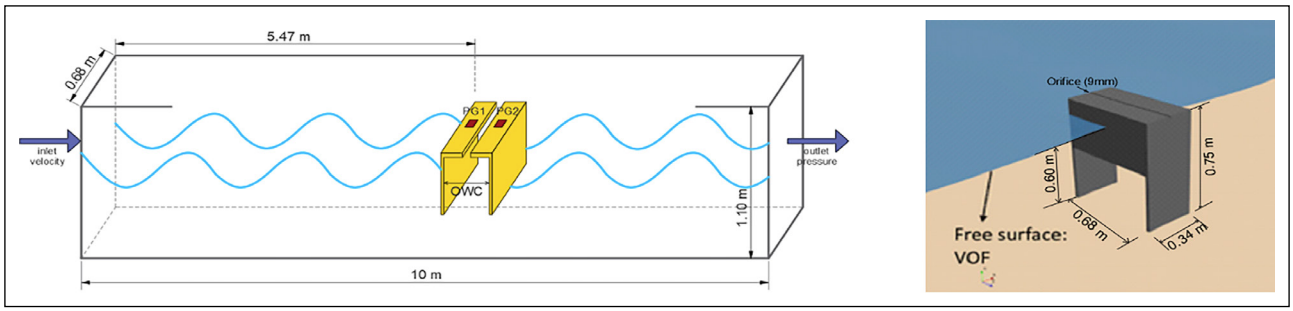

Figure 2. Illustration of the numerical wave tank, and a single OWC model (Iturrioz et al., 2015) view in Simcenter Star CCM+.

To accurately model the flow dynamics surrounding the OWCs, the arrays' solution domain was meticulously constructed in accordance with the previous sections and Table 1. The sections and plan views are for all configurations, with Figure 3 showing an illustration of the array domain for A10 as an example.

2.5. Meshing

The mesh structure was developed using hexahedral grid elements, with volumetric controls implemented in specific regions to generate refinement zones. To enhance the accuracy of the model, particular attention was given to refining the computational mesh surrounding the free surface. Additionally, the mesh has precisely refined the flow around the OWCs to account for high velocity and pressure gradients. Notably, thorough computational modeling of the flow discharge has been achieved by utilizing very thin grid elements in the slot region. Figure 4 depicts the general structure of the volume mesh of an array. The total cell count in the computational array models ranges from 7.0 to 9.8 million cells and vary based on the distance between the geometries.

The accurate representation of free surface waves necessitates high-resolution grid mapping. In cases involving extensive domain dimensions or significant wave heights, the total mesh count might become extremely large to achieve a fine mesh size. Hence, as the total mesh size expands, the required computational resources and solution times also rise. Adaptive mesh refinement (AMR) emerges as a feasible strategy for addressing this issue. AMR enables localized grid refinement in areas of interest by identifying a target scalar and refining the mesh solely in these areas. Additional details regarding the AMR technique can be found in the solver's manual (Siemens Digital Industries Software, 2020).

The current investigation employs an AMR technique to enhance the accuracy of free surface wave representations. Figure 5 highlights the grid structure and AMR visualization. AMR techniques are used to automatically identify the free surface interface and refine the grid around the water-air interface. The refined regions move in conjunction with the free surface every 5 timesteps as the waves progress.

2.6. Energy extraction and efficiency

The average power absorbed by a regular wave is calculated by analyzing the numerical data in the time domain. P_{OWC} is the pneumatic power extracted on a time-averaged basis (Morris-Thomas et al., 2007). P_{inc} refers to the energy flux associated with the incident wave and represents the available power within the wave. The formulations are given as follows:

$$P_{OWC} = \frac{1}{T}\int_0^T \Delta P(t) q(t) dt \tag{3}$$

$\Delta P(t)$ is the differential air pressure and $q(t)$ is the air flow rate, and

$$P_{inc} = \frac{1}{2}\rho_w g {A_i}^2 C_g \tag{4}$$

where A_i is the amplitude of incident wave, and g is the acceleration of gravity. C_g represents group velocity and is formulated as follows:

$$C_g = \frac{\omega}{2k}\left(1 + \frac{2kh}{\sinh(2kh)}\right) \tag{5}$$

Based on Equations 4 and 5, Equation 6 can be obtained as:

$$P_{inc} = \rho g {A_i}^2 \frac{\omega}{k}\left(1 + \frac{2kh}{\sinh 2kh}\right) \tag{6}$$

where g, k, and h are gravitational acceleration, wave number, and fixed water depth, respectively. The dispersion relation is calculated as shown in Equation 7.

$$\omega^2 = gk \tanh(kh) \tag{7}$$

Table 1. Information about wave characteristics and array cases

Array name	Wave height H [m]	Wave period T [s]	Slot size [mm]	OWC geometry	OWC array arrangement
A5	0.08	1.3	9	Rectangular	5D
A10	0.08	1.3	9	Rectangular	10D
B5	0.08	1.3	9	Square	5D
B10	0.08	1.3	9	Square	10D
C5	0.08	1.3	9	Cylindrical	5D
C10	0.08	1.3	9	Cylindrical	10D

OWC: Oscillating Water Column.

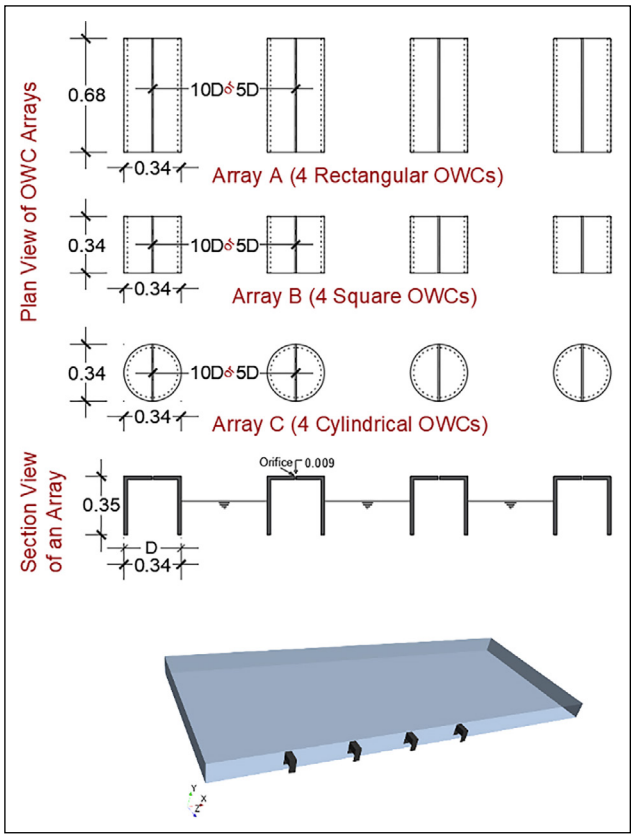

Figure 3. Array plans, section drawings, and model views for Array A10.

The OWC device's hydrodynamic efficiency (η) can be determined by dividing the extracted pneumatic power by the incident wave power, as shown in Equation 8.

$$\eta = {P_{owc}}/{P_{inc}} \tag{8}$$

3. RESULTS AND DISCUSSION

The primary goal of this research is to evaluate the impacts of varying geometric profiles and distance lengths on the generating power and hydrodynamic efficiency of multiple OWCs in an array. After validating the single OWC computational model, a thorough series of numerical simulations was carried out to analyze the fluid dynamics inside the chamber. This has included studying three different chamber shapes (i.e., rectangular, square, and cylindrical), with each used in two different layout configurations.

3.1. The single OWC model

The slot in an OWC system serves as the interface through which air enters and exits the chamber as the water column oscillates, with narrower slots restrict the flow of air through it more. As a result, the velocity of the air passing through the slot increases, leading to higher shear forces and increased viscous damping. Therefore, an increase in damping is observed as the slot of an OWC system becomes thinner. Iturrioz et al.'s (2015) study also highlighted this by comparing chambers' mean pressure oscillation with different top orifice sizes (e.g., 50mm, 9mm, 4.5mm). The current study has chosen the 9mm slot size because of its greater hydrodynamic efficiency. All the experimental data (Iturrioz et al., 2015) about case C24 and its 9mm top slot have been obtained from the wave and pressure gauges. Because the air velocity along the z-axis is the primary driver, it is one of the values utilized to validate the model. Figure 6 presents a comparison of the velocity values, and the well-matched crests and troughs show strong consistency between the air velocities from both the computational model and physical measurements.

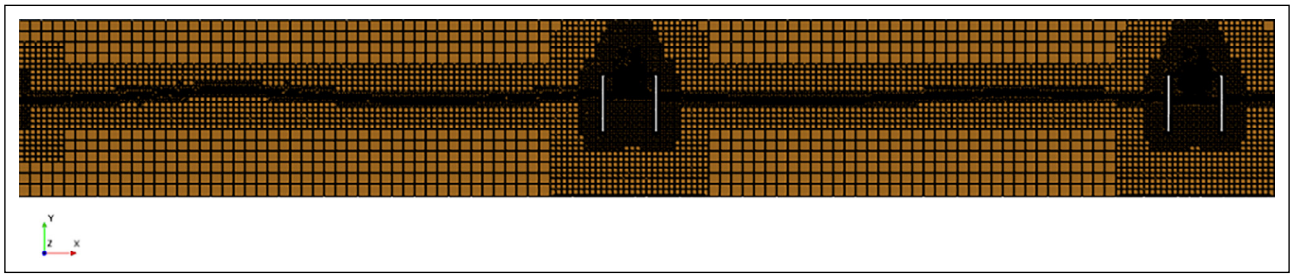

Figure 4. Numerical domain view and mesh generation of array A10.

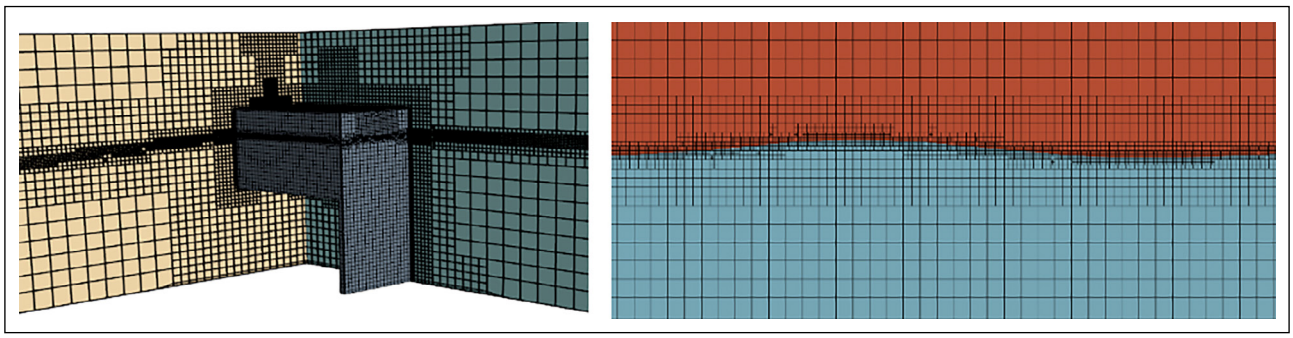

Figure 5. Section view of the grid system and AMR at the free surface.

AMR: Adaptive Mesh Refinement.

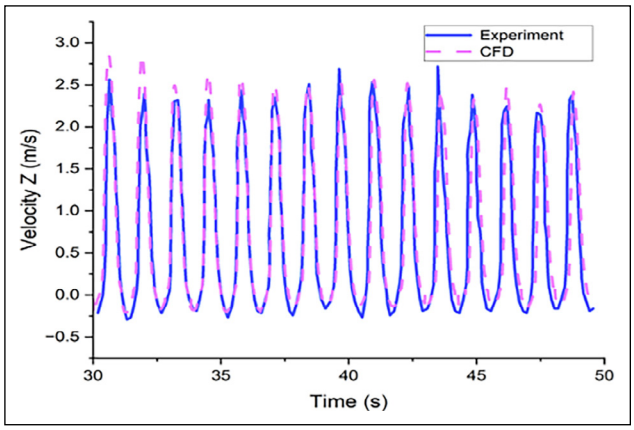

Figure 6. Numerical and experimental comparison of air velocity (Iturrioz et al., 2015) (C24 with 9mm top slot).

CFD: Computational fluid dynamics.

The current numerical model has accurately captured the effective pressure. Figure 7 demonstrates the comparison of ΔP (P_{total}-P_{atm} = $P_{effective}$) between the experimental and numerical results, showing strong agreement.

The oscillating water column wave energy converter is characterized by a repetitive process controlled by the rise and fall of water levels in a chamber. Figures 8a-h show this cycle over a duration of one wave period. When an ocean wave crest approaches the device, the increasing water level in the chamber compresses the air trapped above it, leading to a rise in pressure. This increased air pressure causes air to flow through an orifice (i.e., slot) that directs the compressed air. Subsequently, as the wave trough passes and the water level in the chamber decreases, the air pressure diminishes, permitting external air to enter the chamber through the opening and initiating a new cycle.

Throughout the analysis, the outward (positive) velocity (i.e., pressure) within the chamber was consistently observed to significantly exceed the inward (negative) velocity (i.e., pressure). This phenomenon can primarily be attributed to the placement of the measuring volume above the opening.

3.2. Impact of shape and spacing on array models

This research examines the numerical analysis of six array layout models. Figure 9 presents a comparative overview of the air velocities observed across various OWCs within the array. The results indicate the shape of the OWC to significantly influence air velocity regardless of distance, with square-shaped OWCs demonstrating superior performance compared to cylindrical OWCs. Upon initial evaluation of the OWC at a distance of 10D, a 27% discrepancy in velocity is noted between the square and cylindrical OWCs located in the first row. This discrepancy further increases as the rows progress. Specifically, air movement within square OWCs is observed to be approximately 39%, 45%, and 47% faster than cylindrical OWCs in the 2nd, 3rd, and 4th rows, respectively. When exploring the 5D distance, it becomes evident that while speed may lower in the 3rd and 4th columns, the most significant contrast between the square and cylinder occurs in the 3rd column.

The rectangular OWCs exhibit intermediate velocity characteristics compared to the square and cylindrical variants. However, velocity dynamics change when considering arrays with a 5D distance, displaying a different pattern from those with a 10D distance. The square-shaped OWCs in the 2nd, 3rd, and 4th rows maintain velocity advantages of nearly 23%, 44%, and 31% over their respective cylindrical OWCs. Table 2 also summarizes the velocity values and the differences.

Beyond shape considerations, the optimal spacing between OWCs is row-dependent rather than being uniformly advantageous for both 5D and 10D distances. Figure 10 illustrates that a 5D distance is preferable for the 2nd row but less so for the 3rd row, only to become advantageous again for the 4th row. This observation aligns with average power generation, where the 1st, 2nd, and 4th rows of OWCs in a 5D array outperform those in a 10D array.

Figure 10 depicts how a pattern occurs irrespective of distance length. The 5D distance exhibits a positive tandem effect between adjacent OWCs, increasing power

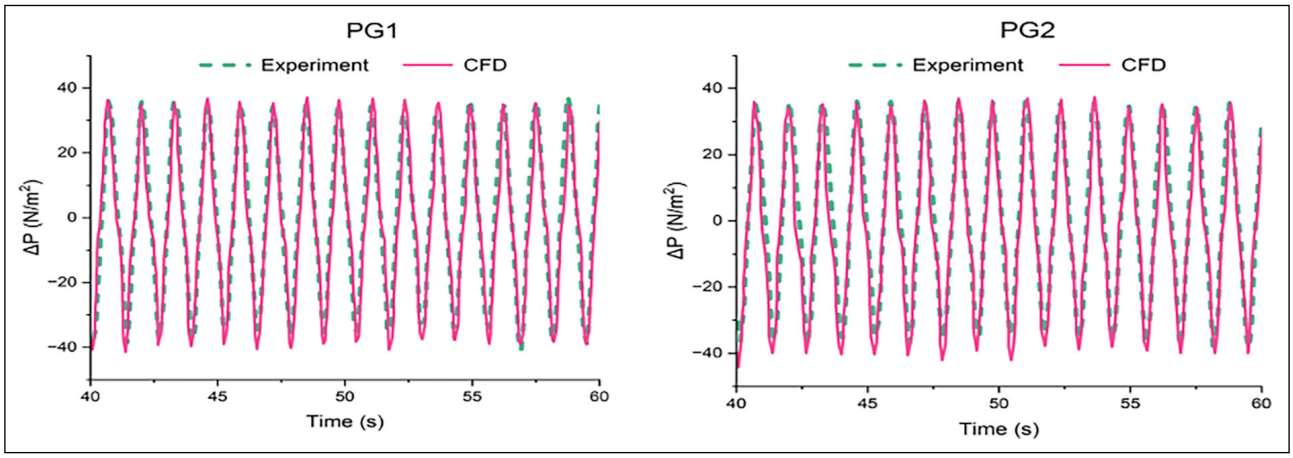

Figure 7. Numerical and experimental comparison of OWC chamber air pressure on a timeline, with the experimental study (Iturrioz et al., 2015) values being for Case 24_9mm top slot.

PG: Pressure gauge; CFD: Computational fluid dynamics; OWC: Oscillating Water Column.

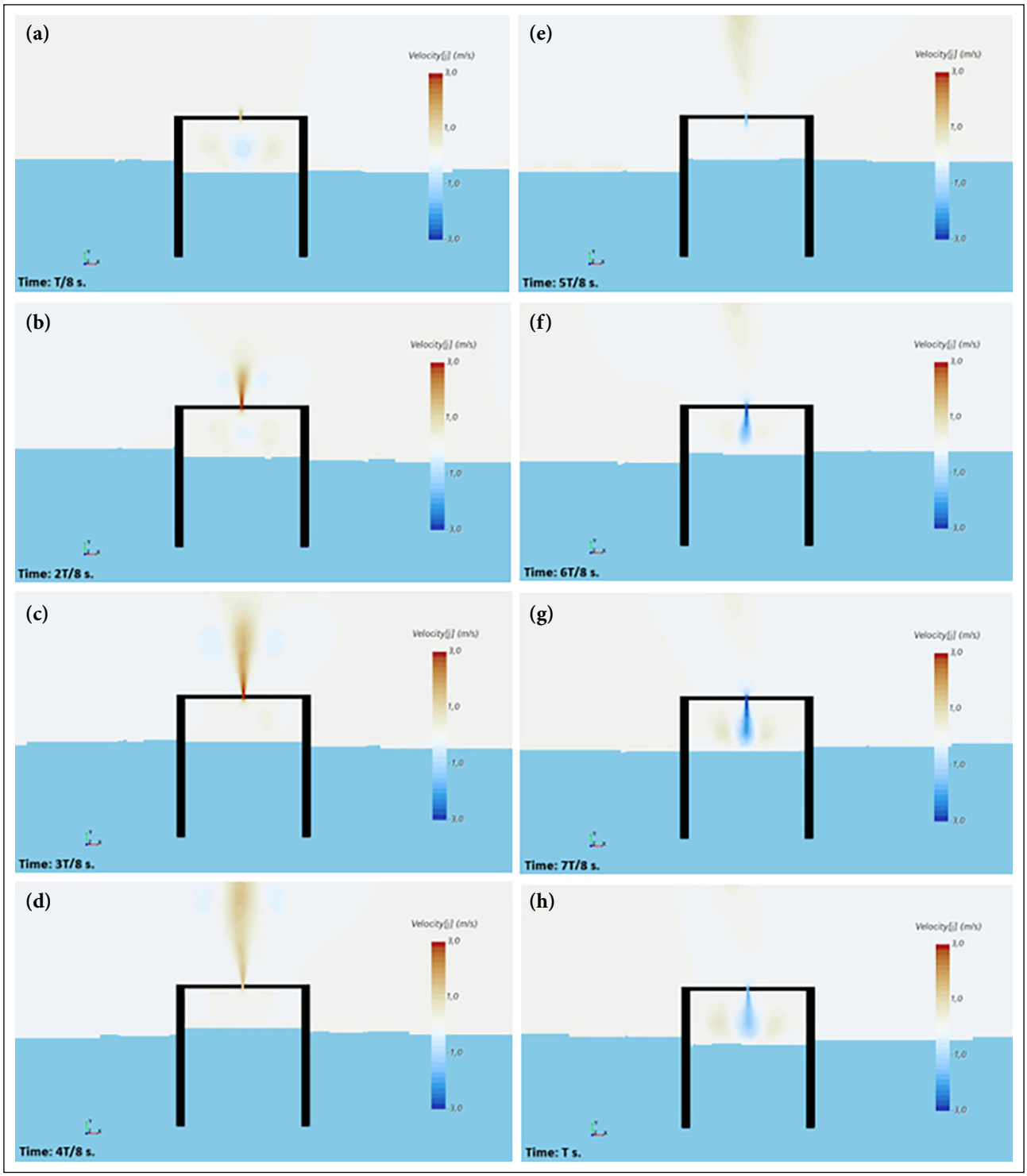

Figure 8. Snapshots (a-h) illustrate air movement of wave period duration through the slot.

generation. In contrast, the impact of a 10D distance varies significantly, with a nearly 40% energy loss observed in the 2nd row, while the 3rd and 4th rows yield comparable average power outputs. The study demonstrates the rectangular-shaped oscillating water column to generate nearly twice the power of the square-type, resulting in a doubling of chamber volume. However, when considering the average power output per unit volume, the square OWC exhibits an almost 10% higher efficiency compared to the rectangular design.

Figure 11 illustrates the hydrodynamic efficiency (η) as a function of dimensionless wave number (*kh*) for each type of OWC. Peak efficiency values consistently occur at a *kh* value of approximately 1.40. Among the OWCs located at a distance of 5D from each other, the 2nd row exhibits the highest efficiency. Specifically, the square type has an efficiency of 0.29, the rectangular type has an efficiency of 0.24 and the cylindrical type has an efficiency of 0.22. All of these forms exhibit efficiencies that are 40-55% higher than those achieved in a 10D space.

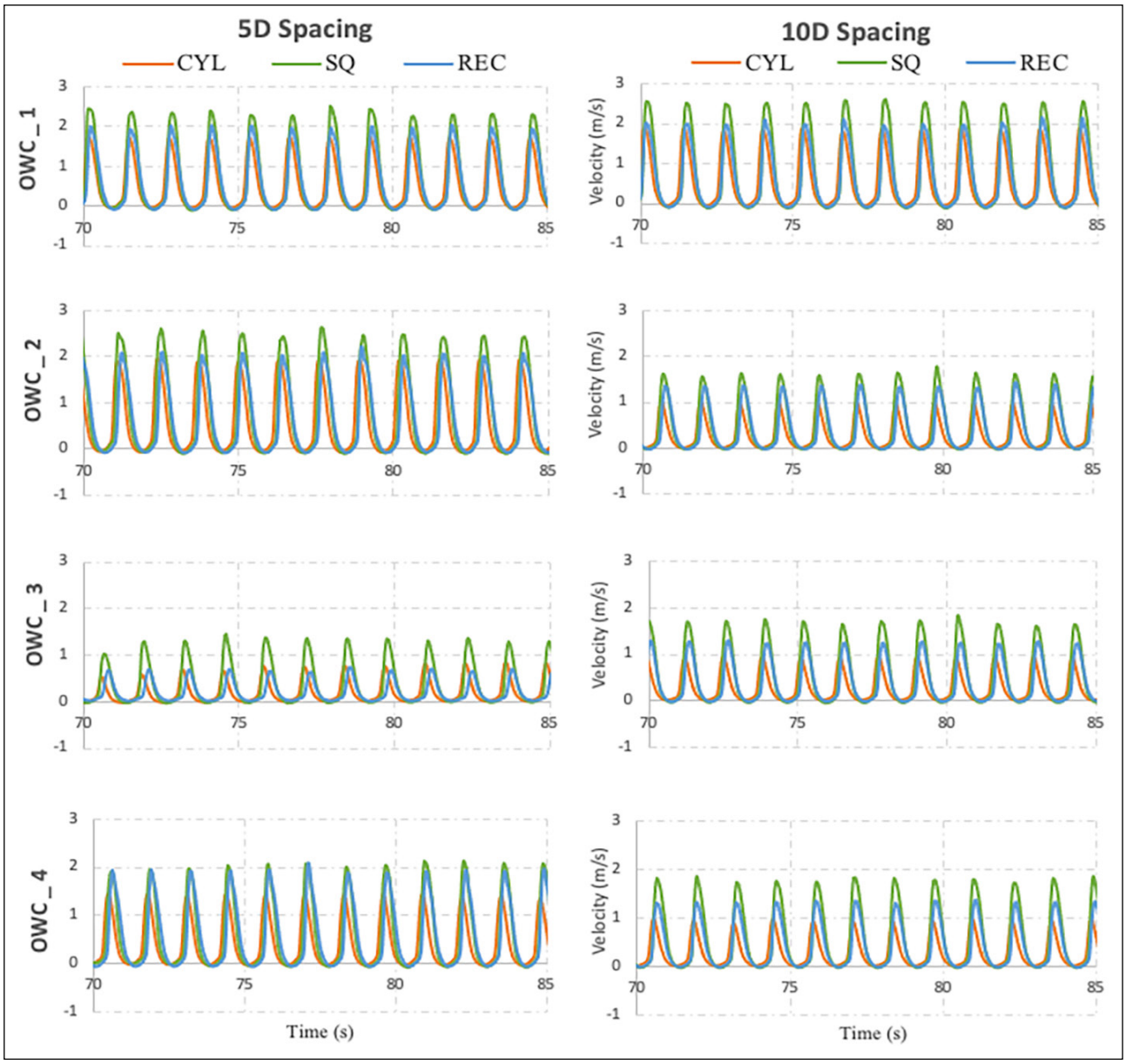

Figure 9. Comparing the velocity values.

CYL: Cylinder; SQ: Square; REC: Rectangle; OWC: Oscillating Water Column.

At a distance of 10D, the most effective devices are located in the initial rows regardless of their shape, as previously indicated. Specifically, square, rectangular, and cylindrical devices exhibit efficiencies of η = 0.27, η = 0.23, and η = 0.21, respectively. After the 1st-row OWC device, efficiency diminishes and remains relatively consistent across the array. The findings are also tabulated in Tables 3 and 4.

Table 2. Summarization of air velocity values for square and cylindrical shapes

OWC type	Distance	OWC 1		OWC 2		OWC 3		OWC 4	
		Max. V	Difference %	Max. V	Difference %	Max. V	Difference %	Max. V	Difference %
Square	10D	2.55	27%	1.64	39%	1.72	45%	1.80	47%
Cylindrical	10D	1.87		0.99		0.94		0.95	
Square	5D	2.36	27%	2.51	2%	1.33	44%	2.05	31%
Cylindrical	5D	1.72		1.93		0.74		1.4	

OWC: Oscillating Water Column; Max. V: Maximum Velocity.

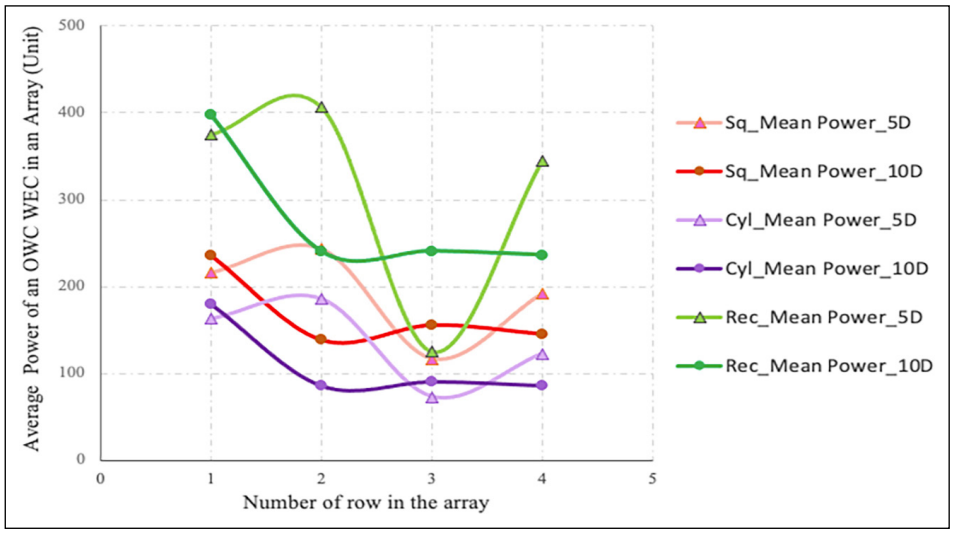

Figure 10. Comparing the mean power for each OWC.

OWC: Oscillating Water Column; WEC: Wave Energy Converter; SQ: Square; CYL: Cylinder; REC: Rectangle.

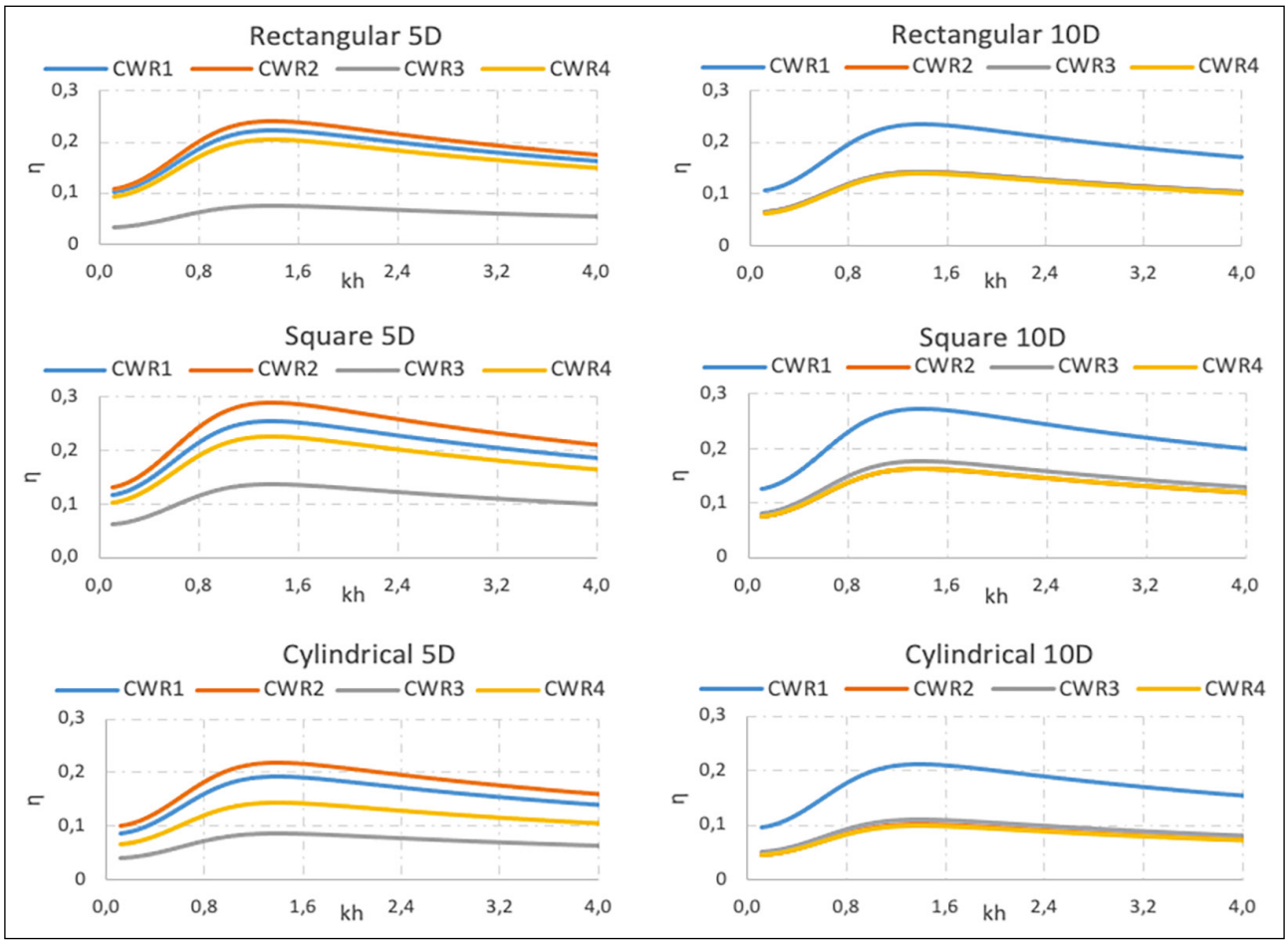

Figure 11. Hydrodynamic efficiency versus dimensionless wave number for all OWCs.

CWR: Capture width ratio; OWC: Oscillating Water Column.

4. CONCLUSION

This study has numerically analyzed OWC WECs under different layout scenarios. These scenarios consist of three different shapes and two different spacing combinations. In total, six configurations have been investigated. The average power was calculated using Equation 3, and hydrodynamic efficiency for each device in the arrays was calculated using Equation 8.

The numerical findings have been validated well in line with the data from Iturrioz et al.'s (2015) experimental study. The study

Table 3. Summarizing the efficiency data for representing the effects of OWC shape

OWC type	Distance	OWC 1		OWC 2		OWC 3		OWC 4	
		η	Difference %	η	Difference %	η	Difference %	η	Difference %
Square	10D	0.27	22%	0.16	38%	0.18	39%	0.16	38%
Cylindrical	10D	0.21		0.10		0.11		0.10	
Square	5D	0.25	24%	0.29	24%	0.14	36%	0.23	35%
Cylindrical	5D	0.19		0.22		0.09		0.15	

OWC: Oscillating Water Column.

Table 4. Summarizing the efficiency data for representing the effects of OWC distances

OWC type	Distance	OWC 1		OWC 2		OWC 3		OWC 4	
		η	Difference %	η	Difference %	η	Difference %	η	Difference %
Square	5D	0.25	7%	0.29	45%	0.14	22%	0.23	30%
Square	10D	0.27		0.16		0.18		0.16	
Cylindrical	5D	0.19	10%	0.22	55%	0.09	18%	0.15	33%
Cylindrical	10D	0.21		0.10		0.11		0.10	
Rectangular	5D	0.22	4%	0.24	42%	0.07	50%	0.20	30%
Rectangular	10D	0.23		0.14		0.14		0.14	

OWC: Oscillating Water Column; η: Efficiency.

used the air velocity in the z direction and pressure difference value at the orifice region, with all visual representations indicating a significant correlation to have been achieved.

The shape of a device is already known to be important for generating power from waves. The working principle of OWC is based on the movement of air and water, so the design of the chamber in which fluids are flowing is crucial. This article has investigated the effect different geometric configurations have on the hydrodynamic effectiveness of the OWC WEC. According to the conducted research, a square shape is shown to be more effective than rectangular or cylindrical shapes, regardless of inter-device distance.

Another important aim of this study has been to observe the relation between the spaces in the layout and generated power. In addition to mean power, the study has also explored efficiency, choosing to investigate inter-device lengths of 5D and 10D. Neither 5D nor 10D can easily be said to perform better, because their performances changed alongside other parameters. However, the OWC in the 2nd row was observed to perform better than the OWC in the first row. This means the OWC in the 2nd row is not affected negatively by the surrounding devices. Meanwhile, the OWC in the 3rd row was greatly affected and generated much less power. The last OWC in the 4th row was again not affected negatively. As demonstrated by the results from the 10D distance, this distance is noted to be large enough not to be affected by the other devices, because after the 1st row, the OWCs in 2nd, 3rd, and 4th rows produced practically the same power. The outcome may not have been optimal under the particular conditions of this study. However, should this unaffectedness continue under real-world sea conditions, then this means any shape could be implemented for OWCs at this distance. Therefore, this distance could be beneficial for maintaining a consistent level of power generation.

The goals and objectives of the research study have been effectively achieved based on the obtained outcomes. This study recommends upcoming research to be able to further refine the design configurations and distances. Future investigations may also involve incorporating actual sea conditions into their analyses.

DATA AVAILABILITY STATEMENT

The published publication includes all graphics and data collected or developed during the study.

CONFLICT OF INTEREST

The author declared no potential conflicts of interest with respect to the research, authorship, and/or publication of this article.

ETHICS

There are no ethical issues with the publication of this manuscript.

USE OF AI FOR WRITING ASSISTANCE

Not declared.

FINANCIAL DISCLOSURE

The authors declared that this study has received no financial support.

REFERENCES

Baudry, V., Babarit, A & Clement, A. H. (2019). *An overview of analytical, numerical and experimental methods for modelling oscillating water columns*. EWTEC, 2013, Aalborg, Denmark. hal-01158853f.

Budal, K. (1977). Theory for Absorption of Wave Power by a System of Interacting Bodies. *Journal of Ship Research, 21*(04), 248–254. [CrossRef]

Doyle, S., & Aggidis, G. A. (2021). Experimental investigation and performance comparison of a 1 single OWC, array and M-OWC. *Renewable Energy, 168*, 365–374. [CrossRef]

Drew, B., Plummer, A. R., & Sahinkaya, M. N. (2009). A review of wave energy converter technology. *Proceedings of the Institution of Mechanical Engineers, Part a: Journal of Power and Energy, 223*(8), 887–902. [CrossRef]

Evans, D. V. (1978). The Oscillating Water Column Wave-energy Device. *IMA Journal of Applied Mathematics, 22*(4), 423–433. [CrossRef]

Evans, D. V. (1979). *Some theoretical aspects of three-dimensional wave-energy absorbers*. Proceeding of the 1st Symposium On Wave Energy Utilization.

Evans, D. V. (1982). Wave-power absorption by systems of oscillating surface pressure distributions. *Journal of Fluid Mechanics, 114*(1), Article 481. [CrossRef]

Falcão, A. F. (2002). Wave-power absorption by a periodic linear array of oscillating water columns. *Ocean Engineering, 29*(10), 1163–1186.

Falcão, A. F. d. O. (2010). Wave energy utilization: A review of the technologies. *Renewable and Sustainable Energy Reviews, 14*(3), 899–918. [CrossRef]

Falcão, A. F., & Henriques, J. C. (2016). Oscillating-water-column wave energy converters and air turbines: A review. *Renewable Energy, 85*, 1391–1424. [CrossRef]

Falnes, J. (2007). A review of wave-energy extraction. *Marine Structures, 20*(4), 185–201. [CrossRef]

Hirt, C., & Nichols, B. (1981). Volume of fluid (VOF) method for the dynamics of free boundaries. *Journal of Computational Physics, 39*(1), 201–225. [CrossRef]

Iturrioz, A., Guanche, R., Armesto, J. A., Alves, M. A., Vidal, C., & Losada, I. J. (2014). Time-domain modeling of a fixed detached oscillating water column towards a floating multi-chamber device. *Ocean Engineering, 76*, 65–74. [CrossRef]

Iturrioz, A., Guanche, R., Lara, J. L., Vidal, C., & Losada, I. J. (2015). Validation of OpenFOAM® for Oscillating Water Column three-dimensional modeling. *Ocean Engineering, 107*, 222–236. [CrossRef]

Konispoliatis, D. N., & Mavrakos, S. A. (2016). Hydrodynamic analysis of an array of interacting free-floating oscillating water column (OWC's) devices. *Ocean Engineering, 111*, 179–197. [CrossRef]

López, I., Andreu, J., Ceballos, S., Martínez de Alegría, I., & Kortabarria, I. (2013). Review of wave energy technologies and the necessary power-equipment. *Renewable and Sustainable Energy Reviews, 27*, 413–434. [CrossRef]

Malmo, O., & Reitan, A. (1985). Wave-power absorption by an oscillating water column in a channel. J*ournal of Fluid Mechanics, 158*, 153–175.

Manimaran, R. (2024). Numerical analysis and performance assessment of trapezoidal oscillating water columns. *Ships and Offshore Structures, 19*(3), 392–408. [CrossRef]

Morris-Thomas, M. T., Irvin, R. J., & Thiagarajan, K. P. (2007). An Investigation Into the Hydrodynamic Efficiency of an Oscillating Water Column. *Journal of Offshore Mechanics and Arctic Engineering, 129*(4), 273–278. [CrossRef]

Nader, J.-R., Zhu, S.-P., Cooper, P., & Stappenbelt, B. (2012). A finite-element study of the efficiency of arrays of oscillating water column wave energy converters. *Ocean Engineering, 43*, 72–81. [CrossRef]

Newman, J. N. (1974). Interaction of water waves with two closely spaced vertical obstacles. *Journal of Fluid Mechanics, 66*(1), 97–106. [CrossRef]

Ning, D.-Z., Shi, J., Zou, Q.-P., & Teng, B. (2015). Investigation of hydrodynamic performance of an OWC (oscillating water column) wave energy device using a fully nonlinear HOBEM (higher-order boundary element method). *Energy, 83*, 177–188. [CrossRef]

O'Boyle, L., Elsäßer, B., & Whittaker, T. (2017). Experimental measurement of wave field variations around wave energy converter arrays. *Sustainability, 9*(1), Article 70. [CrossRef]

Qiao, D., Haider, R., Yan, J., Ning, D., & Li, B. (2020). Review of Wave Energy Converter and Design of Mooring System. *Sustainability, 12*(19), Article 8251. [CrossRef]

Ross, D. (1995). *Power from sea waves*. Oxford University Press.

Siemens Digital Industries Software. (2020). UserGuide Simcenter Star CCM+ Version 2020.1.

Windt, C., Davidson, J., & Ringwood, J. V. (2018). High-fidelity numerical modelling of ocean wave energy systems: A review of computational fluid dynamics-based numerical wave tanks. *Renewable and Sustainable Energy Reviews, 93*, 610–630. [CrossRef]

Yacob, D. H., Sarip, S., Kaidi, H. M., Ardila-Rey, J. A., & Muhammad-Sukki, F. (2022). Oscillating Water Column Geometrical Factors and System Performance: A Review. *IEEE Access, 10*, 32104–32122. [CrossRef]

Zhang, Y., Zhao, Y., Sun, W., & Li, J. (2021). Ocean wave energy converters: Technical principle, device realization, and performance evaluation. *Renewable and Sustainable Energy Reviews, 141*, Article 110764. [CrossRef]

Zhou, Y., Ning, D., Liang, D., & Cai, S. (2021). Nonlinear hydrodynamic analysis of an offshore oscillating water column wave energy converter. *Renewable and Sustainable Energy Reviews, 145*, Article

111086. [CrossRef]

Zhou, Y., Ning, D., Liang, D., & Qiao, D. (2022). Nonlinear wave loads on an offshore oscillating-water-column wave energy converter array. *Applied Ocean Research, 118*, Article 103003. [CrossRef]

Zhou, Y., Ning, D., Shi, W., Johanning, L., & Liang, D. (2020). Hydrodynamic investigation on an OWC wave energy converter integrated into an offshore wind turbine monopile. *Coastal Engineering, 162*, Article 103731. [CrossRef]